Extraction of wave parameters from measured HF radar sea-echo Doppler spectra

Donald E. Barrick

Reprinted from
RADIO SCIENCE
Volume 12 Number 3 May-June 1977

Radio Science, Volume 12, Number 3, pages 415-424, May-June 1977

Extraction of wave parameters from measured HF radar sea-echo Doppler spectra

Donald E. Barrick

Wave Propagation Laboratory, Environmental Research Laboratories, National Oceanic and Atmospheric Administration, US Department of Commerce, Boulder, Colorado 80302

(Received December 6, 1976.)

Computerized techniques for extracting rms wave height and dominant wave period from HF radar sea-echo Doppler spectra are derived. Earlier theoretical models for first- and second-order sea backscatter (derived elsewhere) are employed to obtain the simple, closed-form inversion equations giving these two radar-deduced quantities. The results are general in that no specific models for the radial or azimuthal form of the wave height directional spectrum need be assumed; the resulting formulas are only weakly dependent upon the radar/wind direction. Approximations made in the derivation are stated, and they are ultimately tested by comparing wave heights and periods extracted from the inversion model with the actual values input to the original equations for scatter. The derived relationships are then tested against some eighty hours of radar measurements taken at a variety of frequencies and buoy-measured sea conditions. Theoretically predicted and empirically determined correction factors for wave height and period are in agreement. Finally, the measurements show that when sea wave height is greater than one twentieth of the radar wavelength, wave height extraction (rms) errors are less than 23%, and wave period extraction errors less than 12%.

1. INTRODUCTION

Since the discovery over two decades ago that the simple Bragg-scatter mechanism is responsible for the characteristics of the sea-echo Doppler spectra [*Crombie*, 1955], considerable interest has ensued in the utilization of MF and HF radars, both in the short-range surface-wave mode and in the long-range skywave mode, for the remote sensing of sea state. Theoretical advances since that time have not only accounted for the dominant "first-order" Doppler peaks in the sea echo [*Barrick*, 1972*a*,*b*], but have explained the observed "second-order" continuum around the first-order peaks [*Barrick*, 1972*b*, 1971*b*]. *Hasselmann* [1971] advanced the notion that the second-order Doppler sidebands should be replicas of the wave height nondirectional temporal spectrum. Using only the hydrodynamics portion of the total second-order transfer coefficient, along with a given wave directional model, *Stewart* [1971] obtained an expression (following Hasselmann's suggestion) relating the mean-square wave height to the ratio of the second-order to the first-order echo energy. *Barrick* [1977] derived and evaluated a general expression for finding the wave height nondirectional temporal spectrum from the measured second-order Doppler spectrum—after weighting by a theoretical function and normalization with respect to the first-order echo energy. Of course, the ultimate goal is to invert the general nonlinear integral equation for the complete wave height directional spectrum from the measured second-order echo spectrum. In the subsequent paper in this issue, *Lipa* [1977] presents one approach to this general inversion problem and successfully tests the technique theoretically.

Of all possible simple descriptors of sea state, the rms wave height is perhaps the most useful and important, followed by mean wave direction and dominant wave period (or velocity). By postulating possible models for ocean-wave directionality about the mean wind direction, various investigators [*Long and Trizna*, 1973; *Tyler et al.*, 1974; *Stewart and Barnum*, 1975] have employed measured data to test the accuracy of inferring wind/wave direction from use of the first-order sea-echo only. No one, however, has either derived or tested a general or complete model for extracting wave height and wave period from HF sea-echo records. The present paper presents such a model and tests its accuracy against some eighty hours of HF surface-wave radar observations.

In the next section we set forth and briefly discuss the equations for first- and second-order Doppler spectra in terms of the ocean wave height directional

spectrum. In the following two sections we then obtain simple models for wave height and period based upon these equations for sea echo; these are used to derive theoretical curves relating the radar-deduced wave height/wave period to the true values which were input to the model. A series of surface-wave observations taken with a multifrequency HF radar are then discussed. Using independent observations of the wave parameters, these same parameters are then deduced from the radar sea-echo by computerized algorithms. Comparisons are made to the theoretical predictions, and the variance (and hence rms error) is calculated for these measured parameters based upon the models. Finally, some guidance is given as to where the models can be expected to be acceptably accurate.

2. BACKGROUND SCATTER THEORY

Results for the HF sea-echo Doppler spectrum, to first and second order, have been published elsewhere [*Barrick*, 1972*b*, 1971*b*]. We repeat the results here only to facilitate the derivations and explanations of the inversion techniques that we will apply subsequently to measured data. To first order, the Doppler spectrum (for backscattered, near-grazing, or surface wave incidence conditions, and for the vertical polarization states) can be expressed in terms of the average radar cross section per unit (mean) sea surface area per rad/s bandwidth as

$$\sigma_{(1)}(\omega_d) = 2^7 \pi k_o^4 \sum_{u,l} S_u(\kappa_{rx},\kappa_{ry})\delta(\omega_d \mp \omega_{or}) \qquad (1)$$

where $\bar{\kappa}_r$ is the total radar wavenumber vector, defined as $\bar{\kappa}_r = \bar{k}_s - \bar{k}_i$. The coordinate system selected here has the backscatter wavevector, $\bar{k}_s$, taken at an angle ϕ with respect to the x direction; hence $\bar{k}_i$ lies in the direction $\phi + \pi$, and is identically $\bar{k}_i = -\bar{k}_s$ for backscatter. Therefore, $\bar{\kappa}_r$ becomes $2k_o \cos\phi\hat{x} + 2k_o \sin\phi\hat{y}$, with k_o being the scalar radio wavenumber. The summation convention (u,l) refers to the upper and lower subscripts and signs in the equation. The quantity ω_d is the radian Doppler shift of the received signal, defined as $\omega_d = \omega_s - \omega_i$, with ω_s and ω_i being the radian frequencies of the scattered and incident signals, respectively. The gravity-wave dispersion relation is employed for the definition

$$\omega_{or} = \mathrm{sgn}(\kappa_{rx})(g\kappa_r)^{1/2} = \mathrm{sgn}(2k_o\cos\phi)\,\omega_B$$

where $\omega_B = (2gk_o)^{1/2}$ is referred to as the "Bragg" frequency for first-order scatter, with g being the acceleration of gravity. The expression $\mathrm{sgn}(x)$ is a sign indicator that takes on the values ± 1 depending upon whether x is $\pm$. The average wave height directional spectrum is separated into two components, S_+ and S_-. Each component is symmetric since it represents pure real waves; i.e., $S_\pm(\kappa_x,\kappa_y) = S_\pm(-\kappa_x,-\kappa_y)$. Both components are employed to define a general wave field that propagates over 360° of azimuth; the only restriction used here for convenience is that the wave field peaks in azimuth along the $+x$ direction (when $\kappa_y = 0$). Inasmuch as this is often the wind direction for fully developed seas, ϕ can be thought of as the angle between the radar direction and the wind direction for such situations. The quantity $\delta(x)$ is the Dirac-delta function of argument x.

The corresponding result for second-order sea echo is

$$\sigma_{(2)}(\omega_d) = 2^8 \pi k_o^4 \sum_{u,l}\sum \iint_{-\infty}^{\infty} d^2\bar{\kappa}_1\, |\Gamma_T|^2 \cdot S_\pm(\kappa_{1x},\kappa_{1y})S_\pm(\kappa_{2x},\kappa_{2y})\delta(\omega_d \pm \omega_{o1} \pm \omega_{o2}) \qquad (2)$$

where

$$\bar{\kappa}_1 = (1/2)\bar{\kappa}_r + \bar{\kappa}_l; \quad \bar{\kappa}_2 = (1/2)\bar{\kappa}_r - \bar{\kappa}_l;$$

$$\omega_{o1} = \mathrm{sgn}(\kappa_{1x})(g\kappa_1)^{1/2}; \quad \omega_{o2} = \mathrm{sgn}(\kappa_{2x})(g\kappa_2)^{1/2};$$

$$\Gamma_T = \Gamma_H + \Gamma_{EM}$$

where

$$\Gamma_H = -(i/2)\{\kappa_1 + \kappa_2 + (\kappa_1\kappa_2 - \bar{\kappa}_1 \cdot \bar{\kappa}_2)[(\omega_B^2 + \omega_d^2) + (\omega_B^2 - \omega_d^2)]g/\omega_{o1}\omega_{o2}\}$$

$$\Gamma_{EM} = (1/2)(\kappa_{1x}\kappa_{2x} - 2\bar{\kappa}_1 \cdot \bar{\kappa}_2)/[(\bar{\kappa}_1 \cdot \bar{\kappa}_2)^{1/2} + k_o\Delta)]$$

and where the integration wavevector may be defined as $\bar{\kappa}_l = p\hat{x} + q\hat{y}$. Here, Δ is the normalized electrical impedance for the rough sea surface for vertical polarization at grazing incidence, as defined and derived by *Barrick* [1971*a*]. The coupling coefficients, Γ_H and Γ_{EM}, are obtained from hydrodynamic and electromagnetic theory, respectively; they are derived by expanding the nonlinear equations for the free water surface and the scattered fields into a perturbational series and retaining the second-order terms [*Barrick*, 1972*b*].

As seen from (1) above, the first-order sea-echo Doppler spectrum consists of two impulse functions symmetrically spaced about the carrier frequency, each originating from two sets of wave trains one half the radar wavelength, advancing toward and receding from the radar; this is identically the Bragg-scatter mechanism. In practice, these "spikes" will not be infinite in height. Their widths will be proportional normally to the receiver's spectral processing resolution, and hence their heights will adjust accordingly so that the area under them, as expressed by the factor multiplying the delta function, remains constant as given in (1). This area is proportional to the heights of the two sets of Bragg-scattering waves, as expressed by the two wave height directional spectra factors evaluated at the Bragg wavenumber. Figure 1 shows a measured sea-echo Doppler spectrum at 13.40 MHz, where the first-order peaks are much in evidence; their widths here are proportional to the receiver spectral resolution. (More will be said subsequently about the details of these measurements.)

The second-order Doppler spectrum represented by (2) is a continuous function of frequency, in contrast to the "spiky" nature of the first-order scatter. Equation (2) shows that this is due to a double-interaction process between two sets of ocean waves having wavevectors $\bar{\kappa}_1$ and $\bar{\kappa}_2$. The measured spectrum of Figure 1 shows where this structure appears. It is this second-order sea echo and its more prominent features, when normalized with respect to the first-order sea echo, that we shall employ subsequently to extract wave height and wave period.

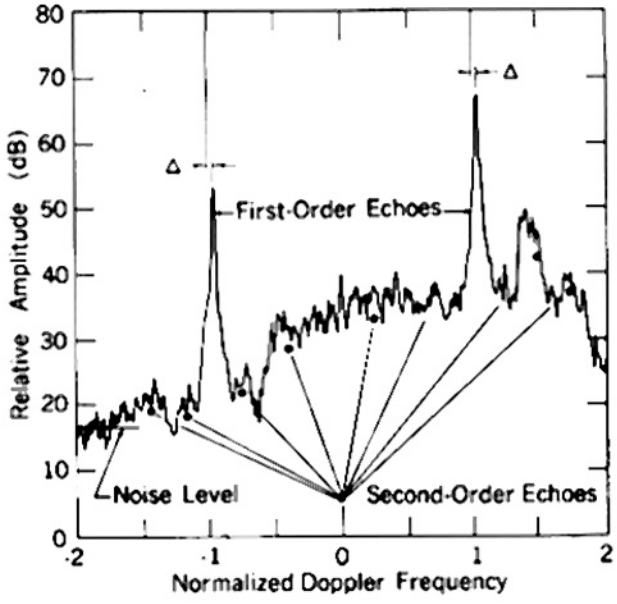

Fig. 1. Measured HF surface-wave sea-echo Doppler spectrum at 13.40 MHz from San Clemente Island.

3. WAVE HEIGHT APPROXIMATION

Hasselmann [1971] initially suggested that the second-order Doppler sidebands around each first-order peak ought to be proportional to the wave height nondirectional temporal spectrum, centered at the first-order Bragg frequency, $\pm\omega_B$. If this were strictly true, the area under these sidebands would be proportional to the mean-square sea wave height. *Stewart* [1971] followed this suggestion to derive a simple proportionality relationship between the mean-square wave height and the ratio between the second-order and first-order spectral energies. However, his model was quite restrictive, based upon (i) neglect of the electromagnetic coupling factor Γ_{EM}; (ii) the assumption of a cosine-square azimuthal model for the wave height directional spectral dependence; and (iii) radar propagation only in the "upwind" direction (i.e., $\phi = 0$ according to our geometry here).

On the basis of these suggestions, we initially attempted (using buoy measurements for wave height "sea truth") to empirically relate the total second-order spectral area, divided by the first-order area, to mean-square waveheight. Furthermore, using the theoretical models above, we derived curves for this relationship as a function of the input wave height and the radar-to-wind direction, ϕ. Although theoretical and experimental results were in reasonably good agreement, the results were rather disappointing for the following reasons: (i) we did not have a simple, closed-form relationship for this area-to-wave height ratio; (ii) both the theoretical curves and the data points appeared to follow a law that could not be described over the region of interest by a simple power-law relationship with a small number of parameters; and (iii) the ratio was highly dependent upon ϕ, the radar-to-dominant-wave direction.

Hence, we derived an approximation on a step-by-step basis, starting from (2), to show that under certain conditions, the concept of forming a ratio

of second-order to first-order energy could be used to obtain wave height. The differences in the approach taken here are: (i) the assumptions required in the approximations we employ are obvious, and the use of these approximations in turn permits us to derive a simple, closed-form result; and (ii) the use of a weighting function for the second-order energy, obtained from the theoretical model, allows the result to be relatively insensitive both to the form of the wave spectrum directionality and to the radar-to-wind direction, ϕ. Details of the steps of the derivation are found in *Barrick* [1977], where the wave height nondirectional temporal spectrum is related to the ratio of the weighted second-order Doppler sidebands to the first-order spectral energy. In this section, we take a different, simple approach to show how one can obtain mean-square wave height; that both analyses lead to the same result will be obvious shortly.

To illustrate the method, let us start from the following integral:

$$I_H = \sum_{n,l}\sum \iint_{-\infty}^{\infty} d^2\bar{\kappa}_l S_{\pm}(\kappa_{1x},\kappa_{1y}) S_{\mp}(\kappa_{2x},\kappa_{2y}) \tag{3}$$

The integrand has two significant regions on the p-q plane: one near $\bar{\kappa}_2 = \bar{0}$ (i.e., at $\bar{\kappa}_l \cong (1/2)\bar{\kappa}_r$), and the other near $\bar{\kappa}_1 = \bar{0}$ (i.e., at $\bar{\kappa}_l \cong -(1/2)\bar{\kappa}_r$). In effect, one wave height spectrum is shifted out from the origin to a new origin at $\bar{\kappa}_2 \simeq \bar{0}$ ($\bar{\kappa}_l = (1/2)\bar{\kappa}_r$), but is weighted and shaped by the other spectrum factor with argument $\bar{\kappa}_1 \cong \bar{\kappa}_r$. Likewise, the other spectrum is located at $\bar{\kappa}_1 = \bar{0}$ ($\bar{\kappa}_l = -(1/2)\bar{\kappa}_r$), but weighted and shaped by the other spectrum with argument $\bar{\kappa}_2 \cong \bar{\kappa}_r$. This is illustrated in Figure 2 by employing a currently popular spectral model $S_{\pm}(\bar{\kappa}) = f(\kappa)g_{\pm}(\theta)$, where $f(\kappa)$ follows the Phillips model for wind-driven, fully developed seas [*Phillips*, 1966], and the directional factor $g_{\pm}(\theta)$ has a form deduced empirically by *Tyler et al.* [1974]. These factors are

$$f(\kappa) = .005/2\pi\kappa^4 \qquad \text{for } \kappa > \kappa_{co} \tag{4}$$

$$g_{\pm}(\theta) = (4/3)\cos^4[\pm|\theta|/2] \tag{5}$$

where $\kappa_{co} \equiv g/u^2$, with g being the acceleration of gravity and u being the wind speed. The original "one-sided" spectrum is shown in Figure 2(a), i.e., $(4/3)f(\kappa)\cos^4(\theta/2)$. Plotted in Figure 2(b) is the symmetricized spectrum $S(\bar{\kappa}) \equiv S_+(\bar{\kappa}) + S_-(\kappa)$ required for real wave fields. Shown then in (c) and (d) are the product functionals (for positive p only, since symmetry obtains for negative p), i.e., $S(\bar{\kappa}_1)S(\bar{\kappa}_2)$. From the definitions following (2) we write this as

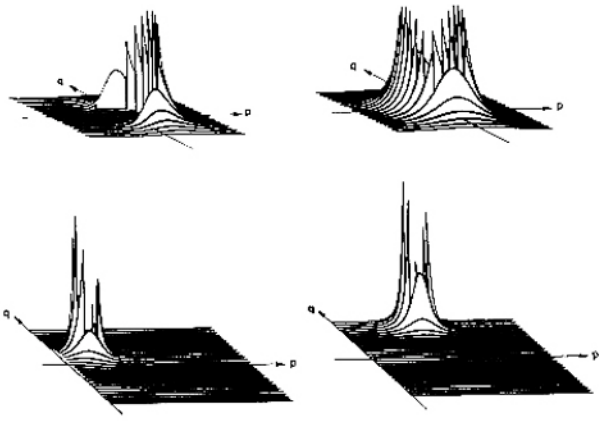

Fig. 2. Three-dimensional plots of single and product wave height directional spectra following (4). Upper left: One-sided spatial spectrum, $S_-(\bar{\kappa})$ for $0 < |\theta| < 90°$ and $S_-(\bar{\kappa})$ for $90° < |\theta| < 180°$. Upper right: two-sided spatial spectrum, $S(\bar{\kappa}) = S_-(\bar{\kappa}) + S(\bar{\kappa})$. Lower left: product functional, $S(\bar{\kappa}_1)S(\bar{\kappa}_2)$ for $\beta/2 = 4$ and $\phi = 45°$. Lower right: product functional, $S(\bar{\kappa}_1)S(\bar{\kappa}_2)$ for $\beta/2 = 10$ and $\phi = 45°$.

$$\begin{aligned} S(\bar{\kappa}_1)S(\bar{\kappa}_2) &= S(\kappa_{1x},\kappa_{1y})S(\kappa_{2x},\kappa_{2y}) \\ &= S(k_o\cos\phi + p, k_o\sin\phi + q) \\ &\cdot S(k_o\cos\phi - p, k_o\sin\phi - q) \\ &= S[(\kappa_{co}\beta/2)\cos\phi + p, (\kappa_{co}\beta/2)\sin\phi + q] \\ &\cdot S[(\kappa_{co}\beta/2)\cos\phi - p, (\kappa_{co}\beta/2)\sin\phi - q] \end{aligned}$$

where $\beta/2 = k_o/\kappa_{co}$ is a dimensionless parameter. As can be seen, this product functional has the effect of taking the single spectrum in (b)—located at $p = q = 0$ and creating two, one located at $p = (\kappa_{co}\beta/2)\cos\phi$, $q = (\kappa_{co}\beta/2)\sin\phi$, and the other at its mirror position $p = -(\kappa_{co}\beta/2)\cos\phi$, $q = -(\kappa_{co}\beta/2)\sin\phi$. Figure 2(c) illustrates this effect for $\beta/2 = 4$ and $\phi = 45°$, while Figure 2(d) has $\beta/2 = 10$ and $\phi = 45°$. At a typical HF radar frequency of 15 MHz, $\beta/2 = 10$ would correspond to an rms wave height of 1.592 m.

The figure demonstrates that as β becomes larger so that the centers of the product-functional spectra move farther apart (as in going from (c) to (d)), the spectrum $S(\bar{\kappa}_2)$ at and near $p = (\kappa_{co}\beta/2)\cos\phi$, $q = (\kappa_{co}\beta/2)\sin\phi$ is "weighted" by an $S(\bar{\kappa}_1)$ which

approaches a constant, i.e.,

$$S(\vec{\kappa}_1) \to S(\kappa_{1x}\beta\cos\phi, \kappa_{1y}\beta\sin\phi) = S(\vec{\kappa}_r)$$

Hence in this limit of large β, we could remove $S(\vec{\kappa}_1)$ from the integrand for positive p, q, giving

$$I_H \cong 2[S_+(\vec{\kappa}_r) + S_-(\vec{\kappa}_r)] \sum_{n,l} \iint_{-\infty}^{\infty} d^2\vec{\kappa}_1 S_z(\kappa_{2x},\kappa_{2y}) \tag{6}$$

The sum/integral factor, however, is identically the mean-square wave height, h_s^2, by definition of a wave height spectrum. Hence we have

$$I_H \cong 2h_s^2[S_+(\vec{\kappa}_r) + S_-(\vec{\kappa}_r)] \tag{7}$$

There are two quantities in the integrand of (2) for $\sigma_{(2)}(\omega_d)$ that keep it from being equal to the I_H of (3): one is the coupling coefficient $|\Gamma_T|^2$, and the other is the δ-function. The former is a function of ω_d and also the integration parameters. We remove it in an approximation that retains its functional dependence on ω_d but averages it over the variable of integration; this defines our dimensionless "weighting function," $w(\nu)$, as [*Barrick*, 1977]:

$$\overline{|\Gamma_T|^2} = (k_o^2/8)w(\nu) \tag{8}$$

where $\nu \equiv \omega_d/\omega_B$ is Doppler frequency normalized to the Bragg frequency. Figure 3 shows a plot of $w(\nu)$ for $0 \le |\nu| \le 2.4$. The singularities at $2^{1/2}$ and $2^{3/4}$ result f om regions of mathematical stationarity which are interpretable physically in terms of the radar/ocean wave interactions; such interpretation is found in *Barrick* [1977].

When (2) is divided by $w(\nu)$ we obtain

$$\frac{\sigma_{(2)}(\omega_d)}{w(\omega_d/\omega_B)} \cong 2^5\pi k_o^4 \sum_{n,l}\sum \iint_{-\infty}^{\infty} d^2\vec{\kappa}_1 S_z(\kappa_{1x},\kappa_{1y}) \cdot S_z(\kappa_{2x},\kappa_{2y})\delta(\omega_d \mp \omega_{o1} \mp \omega_{o2})$$

The δ-function can be eliminated by integrating the entire equation with respect to ω_d, at which point we arrive at (8):

$$\int_{-\infty}^{\infty} \frac{\sigma_{(2)}(\omega_d)}{w(\omega_d/\omega_B)} d\omega_d = 2^5\pi k_o^4 \sum_{n,l}\sum \iint_{-\infty}^{\infty} \cdot d^2\vec{\kappa}_1 S_z(\kappa_{1x},\kappa_{1y}) S_z(\kappa_{2x},\kappa_{2y}) = 2^5\pi k_o^4 I_H \cong 2^6\pi k_o^4 h_s^2[S_+(\vec{\kappa}_r) + S_-(\vec{\kappa}_r)] \tag{9}$$

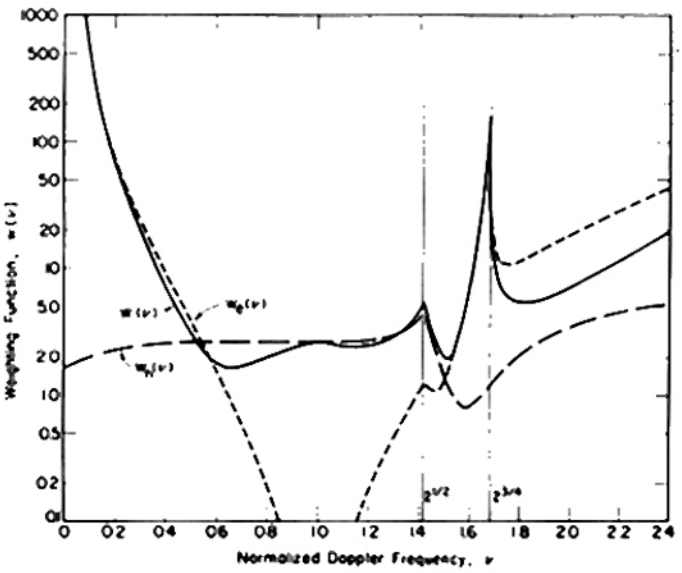

Fig. 3. Weighting function $w(\nu)$ as defined in (8). Also shown are the contributions to this function of the electromagnetic (e) and hydrodynamic terms (h) when each acts alone.

The unknown wave height directional spectrum evaluated at the Bragg radar wavenumber, $\vec{\kappa}_r$, is obtained from the first-order Doppler spectrum, (1), by integrating over ω_d:

$$\int_{-\infty}^{\infty} \sigma_{(1)}(\omega_d)d\omega_d = 2^7\pi k_o^4[S_+(\vec{\kappa}_r) + S_-(\vec{\kappa}_r)] \tag{10}$$

Dividing the two equations gives the desired result:

$$k_o^2 h_s^2 = \frac{2\displaystyle\int_{-\infty}^{\infty} [\sigma_{(2)}(\omega_d)/w(\omega_d/\omega_B)]d\omega_d}{\displaystyle\int_{-\infty}^{\infty} \sigma_{(1)}(\omega_d)d\omega_d} \tag{11}$$

Thus we have shown via two approximations how one can obtain an expression for the radar-deduced mean-square wave height, h_s^2, in terms of the weighted second-order spectral area divided by the first-order area; the validity of those approximations will be tested in a subsequent section. It is not necessary to integrate the spectral quantities in numerator and denominator over the entire Doppler region (i.e., $-\infty < \omega_d < \infty$). Many measured Doppler spectra will have one very strong side, while the other may be uncomfortably near the noise level; in this case, one can integrate both numerator and denominator only over the stronger side (i.e., $-\infty$

$< \omega_d < 0$ or $0 < \omega_d < \infty$). Also, while (11) is given in terms of $\sigma_{(2)}(\omega_d)$ and $\sigma_{(1)}(\omega_d)$, it is not necessary to know the absolute values of these quantities. Any unknown path loss or system gain factors multiplying one will also multiply the other, and the division process removes all such unknown factors. To apply (11) to measured data, it is necessary only that $\sigma_{(2)}$ and $\sigma_{(1)}$ both be identifiable and above the noise level.

4. WAVE PERIOD APPROXIMATION

Barrick [1977] derived an expression, as initially suggested by *Hasselmann* [1971], for the wave height nondirectional temporal spectrum in terms of one of the weighted Doppler second-order sidebands. Again, taking the side with the stronger power density, this expression is:

$$S_t[\omega_B|\nu - 1|] = [4\sigma_{(2)}(\omega_B\nu)/w(\nu)] \Big/ k_o^2 \int_0^\infty \sigma_{(1)}(\omega_d)\mathrm{d}\omega_d \tag{12}$$

where it is assumed that the spectral sidebands from 0 to ∞ are stronger, and that either one of the two sidebands near $\nu = 1$ is used (or better yet, their average).

We define the mean wave frequency in a "centroid" sense, i.e.,

$$\bar{\omega} = \int_0^\infty \omega S_t(\omega)\mathrm{d}\omega \Big/ \int_0^\infty S_t(\omega)\mathrm{d}\omega$$

and its reciprocal as the mean wave period, i.e., $\tau = 2\pi/\bar{\omega}$. Hence, our radar-deduced mean wave period would be

$$\frac{\omega_B \tau_o}{2\pi} = \frac{\displaystyle\int_{0.1}^{1.\infty} [\sigma_{(2)}(\omega_B\nu)/w(\nu)]\mathrm{d}\nu}{\displaystyle\int_{0.1}^{1.\infty} |\nu - 1|[\sigma_{(2)}(\omega_B\nu)/w(\nu)]\mathrm{d}\nu} \tag{13}$$

where again the integrations could run from either 0 to 1 or 1 to infinity.

The mean wave velocity may be defined in terms of this mean wave period obtained from the centroid by using the gravity-wave dispersion equation:

$$v_o = g\tau_o/2\pi \tag{14}$$

5. ACCURACY OF INVERSION MODELS: RECOVERED VS. ORIGINAL PARAMETERS

One method of testing the accuracy of the inversion techniques for wave height, h_o, and wave period, τ_o, and hence the validity of the approximations employed, is to see how well the technique recovers the desired parameter when one uses a known expression for the wave height directional spectrum in the original theoretical expressions, (1) and (2). Thus one knows precisely h and τ corresponding to the wave height directional spectrum used, then obtains $\sigma_{(1)}(\omega_d)$ and $\sigma_{(2)}(\omega_d)$ from (1) and (2), and finally recovers h_o and τ_o from (11) and (13).

To test the inversion models, we employed two different forms for the radial wavenumber dependence of the wave height spectrum, $f(\kappa)$ (as defined in connection with (7)). One was the Phillips model with the sharp cutoff for fully developed seas, as given in (7); the κ^{-4} spatial wavenumber dependence of this spectrum in the equilibrium region in turn transforms (via the first-order gravity-wave dispersion relation) to an ω^{-5} temporal frequency dependence. In addition, we employed a truncated version of the Phillips temporal spectrum, such that this model followed the ω^{-5} dependence for $\omega > 2^{1/2}\,\omega_{co}$, was flat for $\omega_{co} < \omega < 2^{1/2}\,\omega_{co}$, and zero for $\omega < \omega_{co}$ ($\omega_{co} \equiv (g\kappa_{co})^{1/2} = g/u$); the latter model would be more representative of seas that have not yet reached full development. In addition, we employed the $\cos^4 \theta/2$ directional dependence given in (5) and three different radar/wind directions: $|\phi| = 0°$, 45°, and 90° (by symmetry, identical results are obtained for $|\phi| =$ 180°, 135°, and 90°).

Initially, we derived values of h_o and τ_o from the inversion models (11) and (13) as functions of $\beta(=2k_o/\kappa_{co})$ for the three values of ϕ. We found, however, from comparing results for the sharply cutoff spectrum with those for the truncated spectrum that a more universal parameter than β is (normalized) wave height, either $k_o h$ (actual rms wave height) or $k_o h_o$ (radar-deduced rms wave height). *In fact, the results to be presented here are independent of whether the spectrum is sharp or flat-topped if they are plotted as functions of* $k_o h_o$. This means in effect that the expressions for radar-deduced wave height and wave period do *not* depend upon the shape (or stage of development) of the spectrum, a fact that confirms the

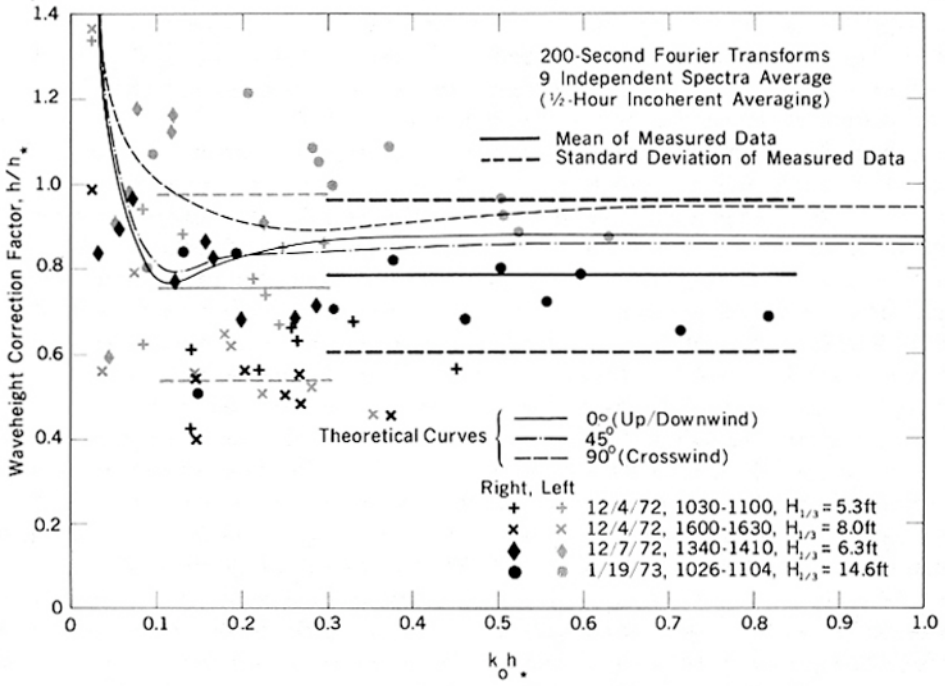

Fig. 4. Theoretical and experimental results of use of wave height inversion model; h_* is radar-deduced rms wave height, using (11), while h is actual (or buoy-measured) wave height.

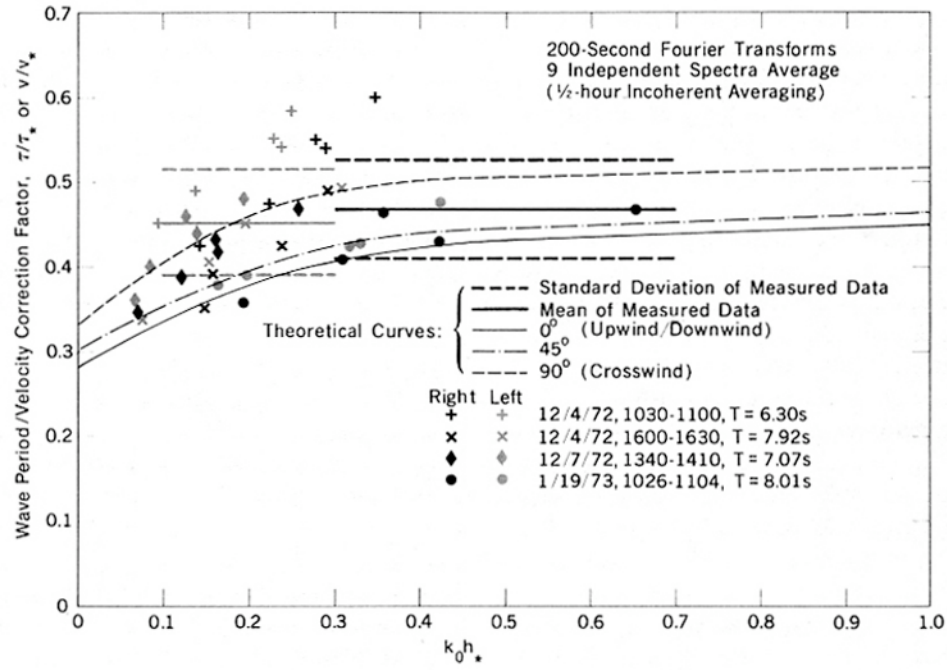

Fig. 5. Theoretical and experimental results of use of wave period inversion model; τ_* is radar-deduced mean wave period, using (13), while τ is actual (or buoy-measured) wave period.

general nature of the technique as derived in the mathematics.

In Figure 4, therefore, we plot h/h_* recovered from (11) as a function of $k_o h_*$ for the three values of radar look direction, ϕ. These curves represent correction factors by which one must multiply the radar-deduced wave height, h_*, in order to obtain the actual wave height (i.e., the input to the models here). Note that the rapidly diverging region for low values of $k_o h_*$ (i.e., $k_o h_* < .15$) implies that the approximations break down for low sea states and/or radar frequencies, as anticipated earlier. Secondly, note that while the curves do not converge exactly to unity for $k_o h_* \to \infty$, their asymptotes always lie closer to unity than 15%. Finally, we note that there is some small directional ϕ-dependence to the curves; this theoretical dependence is not nearly so pronounced, however, as it was when we did not weight the second-order Doppler spectra.

The curves for τ/τ_* do appear to approach unity asymptotically (Figure 5) for large $k_o h_*$. Again, the "sharp" and the "truncated" Phillips models gave the same correction curves for Figure 5, validating our use of the independent variable $k_o h_*$.

In theory then, one would employ the following steps to deduce precisely h and τ, the wave height and wave period: (i) Determine (if possible) the direction ϕ by using an alternate, independent technique (such as those described by *Long and Trizna* [1973], *Tyler et al.* [1974], or *Stewart and Barnum* [1975]). (ii) Determine h_* using (11). (iii) Enter the graph of Figure 4 with the values for ϕ and $k_o h_*$, obtaining the correction factor for converting h_* to h. (iv) Determine τ_* using (13). (v) Enter the graph of Figure 5 with the values for ϕ and $k_o h_*$, obtaining the factor for converting τ_* to τ.

If one does not know the radar look direction, ϕ, the figures give a range of uncertainty for the desired wave parameters, h and τ, which, as illustrated in the figures, is not all that great anyway. Hence for many applications, it may be just as convenient to ignore the dependence on ϕ in order to simplify the approach.

6. MEASURED DATA

HF surface-wave sea-echo measurements were made at a radar facility located on the west coast of San Clemente Island in late 1972 and early 1973. The system was built by the Institute for Telecommunication Sciences of the US Department of Commerce and was operated under contract with the Wave Propagation Laboratory for this series of measurements.

Surface-wave radar data were obtained simultaneously at 10 frequencies extending from about 2.4 to 25 MHz. Receiver range gates were set to sample cells centered 22.5, 30.0, and 37.5 km from the radar. The receiving antenna consisted of an array of 13 monopoles phased and switched to alternately produce two beams each having a nominal beamwidth of 10° centered at azimuth angles of 240° and 270°. The combination of 10 frequencies, 3 ranges, and 2 antenna beams resulted in a total of 60 different data samples being recorded.

The transmitting antenna was a two-bay, vertically polarized, log-periodic antenna having a nominal half-power beamwidth of 60° over the HF band. Since this beamwidth illuminated both sectors covered by the receiving beams, no transmitter antenna steering was used. Power patterns of both receiving and transmitting antennas were measured from a small boat to verify gain and beamwidth performance. Radar characteristics are summarized in Table 1.

An on-line computer processed the received signals and computed the power spectrum for each of the 60 data channels. The power spectra that were processed on-line were calculated from signals that had been coherently sampled over a 200-sec window. Since a typical measurement period was 30 min, a total of 9 spectra would be computed during this time. These power spectra and the unprocessed IF data were recorded on magnetic tape to permit subsequent off-line analysis.

Wave heights and periods were measured

TABLE 1. Summary of San Clemente Island surface-wave radar characteristics.

Operating frequency range	2 to 25 MHz
Range gate distances	22.5, 30.0, 37.5 km
Available pulse lengths	20, 50, 100 μs (3.0, 7.5, 15.0 km)
Pulse repetition frequency	20 Hz per frequency
Transmitter peak power	40 kw
Antenna beamwidths	
Receiving (2 beams)	10° at 240° and 270° azimuth
Transmitting	60° at 255° azimuth
Antenna gain product	18 dB at center of HF band decreasing to 0 dB at band edges

independently by a Waverider Data Buoy moored 29.4 km from the radar site on an azimuth of 240°. These values of h and τ, taken here as the "sea truth," were confirmed (to ~10%) by comparisons with hindcasts from surface winds made over the same area and for the same time periods. Data from four different days were selected because of the fairly wide range of sea states and stages of development for these days. Because of the difficulty involved, no attempt was made to (directly) measure the dominant wave direction, ϕ, with respect to the radar look direction.

Computerized algorithms based on the use of (11) and (13) were developed to automatically extract wave height, h_s, and period, τ_s, from sample-averaged Doppler spectra such as those of Figure 1. First of all, the algorithm locates the first-order echo peaks. By searching for the nulls on either side of the dominant first-order peak, the algorithm identifies and separates the first-order echo from the second-order echo. To illustrate with an example, the remaining second-order echo after the first-order positive peak is removed from Figure 1 is shown as the solid curve of Figure 6. The computer then divides this second-order spectral energy by the weighting function, $w(\nu)$; the result is shown as the dotted curve of Figure 6. Finally, integrating both the weighted second-order energy and the first-order energy, as called for in (11) and (13), values for $k_o h_s$, h_s, and τ_s are obtained at the different frequencies, sea states, range gates, and beam positions. Knowing the buoy-measured values of h and τ, the resulting points were then plotted on Figures 4 and 5. Again, uncertainty regarding sea wave direction, ϕ, makes it impossible to identify the points with regard to this parameter. Over eighty hours of observations are represented by the data points on these plots.

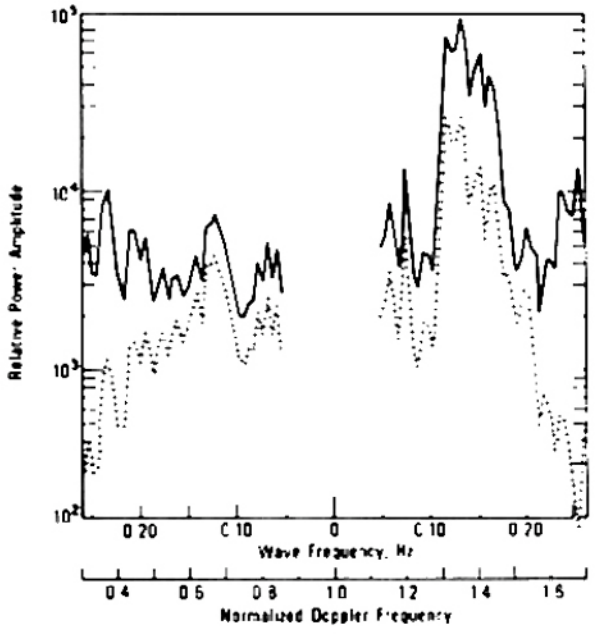

Fig. 6. Example from Figure 1 showing second-order portion of Doppler spectrum on positive side before weighting (solid) and after weighting (dotted).

The measured data points show a greater spread at the lower end, where the theoretical curves indicate that the approximations employed should be least valid. Consequently, we have calculated and shown the means and standard deviations over two regions of $k_o h_s$: for $0.1 < k_o h_s < 0.3$ and for $0.3 < k_o h_s < \infty$. For $k_o h_s > 0.3$, the empirically determined mean wave height correction factor is 0.785 and the mean wave period correction factor is 0.935. As can be seen, these are consistent with the theoretically deduced correction factors in each case. The percentage error for $k_o h_s > 0.3$, defined as the standard deviation of the measured data points divided by their mean, is 22.7% for wave height and 12.4% for wave period.

7. DISCUSSION AND CONCLUSIONS

This paper has concentrated upon developing and testing (against measured surface-wave sea echo) simple, closed-form models for estimating wave height and wave period with an HF radar. Unlike techniques described in the literature [*Long and Trizna*, 1973; *Tyler et al.*, 1974; *Stewart and Barnum*, 1975] for deducing mean wave direction, the methods described here are *not* based on the assumption of a given model for either the azimuthal directionality or the radial wavenumber dependence of the wave height directional spectrum. A goal here also was to obtain a simple inversion scheme that does not require *a priori* knowledge of the angle, ϕ, between the radar and mean wave direction.

Both theoretical predictions and measured data show that one can deduce both wave height and wave period reasonably accurately, so long as the parameter $k_o h_s$ is greater than 0.1. Measured data show that for $k_o h_s > 0.3$, wave height, h, can be deduced to an rms accuracy of ~23%, while wave period, τ, to an accuracy of ~12%. Theoretical

predictions show that part of this spread or error is due to the dependence of the results on the radar look angle, ϕ. Thus if one wishes to obtain better accuracy, he should employ alternate techniques to estimate ϕ, and then use this information, along with the curves of Figures 4 and 5, to find a closer estimate for the required correction factor. Hence the accuracies quoted above apply for the crudest and simplest inversion process, where one does not wish to bother with direction in order to estimate wave height and period. The models are straightforward, closed-form equations requiring measurement of the HF sea-echo Doppler spectrum and the use of a simple dimensionless weighting function presented here in Figure 3; the latter is a single curve over Doppler frequency, which is independent of radar frequency, look direction, wave height, or any other parameter. Obviously, further simplification is possible if one is willing to treat the weighting function as a constant over the region of greatest importance ($0.5 \leq |\nu| \leq 1.5$); how much further error such a simplification will produce has not been studied here.

Several things could degrade further the accuracy in estimating these parameters from measured data. Poor system Doppler resolution will produce some error; the above accuracies should apply if one can realize a Doppler resolution (at mid-HF) of ~0.02 Hz or better, requiring a 50-sec coherent processing period or longer. Inadequate incoherent averaging will also produce some error. With processing times exceeding 50 sec, one cannot afford to add hundreds of sequentially measured spectra to obtain an average. Thus a sample average of, say, ten Doppler spectra will still be somewhat random in appearance; curves for the confidence vs. number of samples for HF Doppler spectra were presented by *Barrick and Snider* [1977]. External (atmospheric) additive noise at HF will result in further error in the use of any inversion techniques such as this when the noise level is significant compared with the echo. This happens, for example, with surface-wave radars for operations at higher frequencies and at greater distances. For skywave radars (using ionospheric reflections), higher additive noise often contaminates the data at nighttime. Finally, skywave radar propagation often smears the dominant features of the Doppler spectra because of turbulence in the reflecting ionospheric layers. This has the effect of reducing the effective Doppler resolution of the received spectra, and can be so bad at times that it is not possible to distinguish the first-order from the second-order portions of the signal spectrum. We and others are presently engaged in extending these methods and developing new techniques to handle such cases of severe ionospheric signal distortions.

Acknowledgments. The author is grateful to J. B. Snider and E. Fenstermacher of our laboratory for their assistance in obtaining and reducing the experimental data. Constructive discussions with B. J. Lipa of Stanford University helped solidify the inversion techniques tested and presented here.

REFERENCES

Barrick, D. E. (1971*a*), Theory of HF/VHF propagation across the rough sea, 1 and 2, *Radio Sci.*, *6*, 517-533.

Barrick, D. E. (1971*b*), Dependence of second-order sidebands in HF sea echo upon sea state, paper presented at IEEE G-AP International Symposium, Los Angeles, California, September 1971.

Barrick, D. E. (1972*a*), First-order theory and analysis of MF/HF/VHF scatter from the sea, *IEEE Trans. Antennas Propagat.*, *AP-20*, 2-10.

Barrick, D. E. (1972*b*), Remote sensing of sea state by radar, in *Remote Sensing of the Troposphere*, edited by V. E. Derr, chap. 12, US Government Printing Office, Washington, DC.

Barrick, D. E. (1977), The ocean wave height nondirectional spectrum from inversion of the HF sea-echo Doppler spectrum, *Remote Sensing Environ.*, in press.

Barrick, D. E., and J. B. Snider (1977), The statistics of HF sea-echo Doppler spectra, *IEEE Trans Antennas Propagat.*, *AP-24*, 19-28.

Crombie, D. D. (1955), Doppler spectrum of sea echo at 13.56 Mc/s, *Nature*, *175*, 681-682.

Hasselmann, K. (1971), Determination of ocean wave spectra from Doppler radio return from the sea surface, *Nature Phys. Sci.*, *229*, 16-17.

Lipa, B. (1977), Derivation of directional ocean-wave spectra by integral inversion of second-order radar echoes, *Radio Sci.*, *12*, this issue.

Long, A. E., and D. B. Trizna (1973), Mapping of North Atlantic winds by HF radar sea backscatter interpretation, *IEEE Trans. Antennas Propagat.*, *AP-21*, 680-685.

Phillips, O. M. (1966), *Dynamics of the Upper Ocean*, pp. 109-139, Cambridge University Press, London.

Stewart, R. H. (1971), Higher-order scattering of radio waves from the sea, paper presented at IEEE G-AP International Symposium, Los Angeles, California, September 1971.

Stewart, R. H., and J. R. Barnum (1975), Radio measurements of oceanic winds at long range: An evaluation, *Radio Sci.*, *10*, 853-857.

Tyler, G. L., C. C. Teague, R. H. Stewart, A. M. Peterson, W. H. Munk, and J. W. Joy (1974), Wave directional spectra from synthetic aperture observations of radio scatter, *Deep Sea Res.*, *21*, 989-1016.